Transonic flow simulations using wall functions

P. Catalano⋆
⋆*Italian Aerospace Research Center*
Via Maiorise, 81043 Capua (CE), Italy

Abstract

This paper presents simulations of the transonic flow around an airfoil and a wing using a wall-functions formulation and no-slip boundary conditions. The aim is to evaluate the accuracy of a wall-function approach for severe transonic applications with flow separation and re-attachment. The wall functions are applied with different turbulence models on either fine and coarse grids. The results are presented with reference to wall-integrated simulations and certified experimental data.

1. Introduction

The wall functions allow to relax the grid requirements of a Navier Stokes simulation. In fact, wall-bounded flows require a mesh-resolution able to resolve the strong gradients of the fluid dynamic variables that occur close to a solid boundary. This paper presents the application of a wall function formulation to the flow around the RAE 2822 airfoil and the wing RAE M2155. Both the applications present a strong boundary layer interaction with a flow separation. Several grids are generated, starting from a fine mesh and increasing the height of the wall-adjacent cells. Different turbulence models are used. The simulations are performed by applying either the wall-functions and no-slip boundary conditions.

2. Formulation

The evaluation of the viscous fluxes of the Navier-Stokes equations envolves the computation of the stress tensor t_{ij} that requires the determination of the velocity derivatives The wall functions allow to obtain the wall stresses avoiding the calculations of the velocity derivatives.

Let us consider a global cartesian reference system $x_i = (x_1, x_2, x_3)$ and a local reference system $\xi_i = (\xi_1, \xi_2, \xi_3)$, the stress tensor can be written as :

$$t_{ij} + \tau_{ij} = \left(\mu + \mu_t\right)\left(\frac{\partial u_i}{\partial \xi_k}\frac{\partial \xi_k}{\partial x_j} + \frac{\partial u_j}{\partial \xi_k}\frac{\partial \xi_k}{\partial x_i} - \frac{2}{3}\frac{\partial u_l}{\partial \xi_m}\frac{\partial \xi_m}{\partial x_l}\delta_{ij}\right) - \frac{2}{3}\kappa\delta_{ij} \tag{1}$$

At the wall the derivatives of the velocity in the stream-wise (ξ_1) and span-wise (ξ_3) direction are zero for the no-slip condition, and only the molecular part of the stress tensor has to be considered because the turbulent velocity fluctuations and hence the eddy viscosity go to zero. Therefore at a solid boundary, equation (1) reduces to

$$t_{ij} = 2\mu\left(\frac{\partial u_i}{\partial \xi_2}\frac{\partial \xi_2}{\partial x_j} + \frac{\partial u_j}{\partial \xi_2}\frac{\partial \xi_2}{\partial x_i} - \frac{1}{3}\frac{\partial u_l}{\partial \xi_2}\frac{\partial \xi_2}{\partial x_l}\delta_{ij}\right)_w \tag{2}$$

A wall function formulation provides a relation between the velocity derivatives and the wall shear stress τ_w as :

$$\tau_{wi} = \mu\left(\frac{\partial u_i}{\partial \xi_2}\right)_{\xi_2=0} = -\rho u_{\tau i}^2 \tag{3}$$

The equation (3) requires the evaluation of the component of the friction velocity $u_{\tau i}$ that, following the relation that holds in the logarithmic region of a turbulent boundary layer can be written as

$$u_{\tau i} = \frac{u_{ti}}{\frac{1}{\kappa_a}\log(\xi_2^+) + B} \tag{4}$$

where u_{ti} are the components, in the global reference system, of the tangential velocity vector, κ_a the von Kármán constant and $B \approx 5$. The distance from the wall is expressed in plus units and depends on the friction velocity

$$\xi_2^+ = \frac{\xi_2 u_\tau}{\nu} \tag{5}$$

where ν is the kinematic molecular viscosity. The equation (4) is solved iteratively and the starting value for the velocity scale [6] is derived from the solution of the turbulent kinetic energy κ as

$$u^* = \beta^{*0.25}\sqrt{\kappa} \tag{6}$$

with $\beta^* = 0.09$, and, as a consequence

$$\xi_2^* = \frac{\xi_2 u^*}{\nu} \tag{7}$$

The equations (6) and (7) allow to address the singularity of equation(4) close to separaton or reattachement points where τ_w and hence u_τ and hence ξ_2^+ goes to zero.

The first layer of cells close to a solid boundary is assumed to have a distance from the wall, always in plus unit, not lower than the intersection between the viscous and logarithmic regions of a boundary layer [7]

$$\xi_2^+ = \frac{1}{\kappa_a}\log(\xi_2^+) + B \Longrightarrow \tilde{\xi}_2 = 11.067 \tag{8}$$

and the (4) is changed to

$$u_{\tau,i} = \frac{u_{ti}}{\frac{1}{\kappa_a}\log(\tilde{\xi}_2^{\,*}) + B} \tag{9}$$

with $\tilde{\xi}_2^{\,*} = \max\left[\xi_2^*, \tilde{\xi}_2\right]$. In order to take into account the effect of the viscous layer, the friction velocity is computed by performing a blending between the viscous and the log layer solutions as

$$u_{\tau,i} = \left[\left(u_{\tau,i}^{visc}\right)^4 + \left(u_{\tau,i}^{log}\right)^4\right]^{0.25} \tag{10}$$

The equation (3) in then changed to

$$\tau_{wi} = \mu\left(\frac{\partial u_i}{\partial \xi_2}\right)_{\xi_2=0} = -\rho u_{\tau,i}\max\left[u_{\tau,i}, u^*\right] \tag{11}$$

2.1 Viscous Forces

In order to compute the viscous forces acting on a surface, the surface stress defined as

$$\underline{t}_n = \underline{n}\cdot\underline{\underline{t}} \tag{12}$$

with n the normal vector, needs to be computed. Equation (12) can be written as

$$t_{n_j} = n_i t_{ij} \tag{13}$$

with t_{ij} given by (2). The surface stress can be written as

$$t_{n_j} = \mu\left[\frac{\partial u_j}{\partial \xi_2} + \frac{1}{3}\frac{S_j}{S}\left(\frac{\partial u_i}{\partial \xi_2}\frac{S_i}{S}\right)\right]_w \tag{14}$$

with S_i the component of the area vector of the face of a computational cell. The components in direction tangent to the surface are given by

$$t_{nt_j} = t_{n_j} - \left(t_{n_i}n_i\right)n_j = \mu\left[\frac{\partial u_j}{\partial \xi_2} - \frac{1}{3}\frac{S_j}{S}\left(\frac{\partial u_i}{\partial \xi_2}\frac{S_i}{S}\right)\right]_w \tag{15}$$

The components of the skin friciton are therefore

$$C_{f_i} = \frac{t_{nt_i}}{\frac{1}{2}\rho_\infty V_\infty^2} \tag{16}$$

It is worth noting that t_{nt_i} reduces to $\tau_{w,i}$ for an incompressible flow.

2.2 Integration of the Turbulence Equations

The transport equation for the turbulenct kinetic energy is solved by applying a Neumann condition at a solid boundary

$$\left.\frac{\partial \kappa}{\partial \xi_2}\right|_{\xi_2=0} = 0 \tag{17}$$

The prodution of the turbulent kinetic energy is given by

$$P_\kappa = \tau_{ij}\frac{\partial u_i}{\partial x_j} \tag{18}$$

which, at a solid boundary, can be written as

$$\begin{aligned} P_\kappa \;=\;& \tau_{11}\frac{\partial u_1}{\partial \xi_2}\frac{S_1}{S} + \tau_{22}\frac{\partial u_2}{\partial \xi_2}\frac{S_2}{S} + \tau_{33}\frac{\partial u_3}{\partial \xi_2}\frac{S_3}{S} + \tau_{12}\Big(\frac{\partial u_1}{\partial \xi_2}\frac{S_2}{S} + \frac{\partial u_2}{\partial \xi_2}\frac{S_1}{S}\Big) + \\ +\;& \tau_{13}\Big(\frac{\partial u_1}{\partial \xi_2}\frac{S_3}{S} + \frac{\partial u_3}{\partial \xi_2}\frac{S_1}{S}\Big) + \tau_{23}\Big(\frac{\partial u_2}{\partial \xi_2}\frac{S_3}{S} + \frac{\partial u_3}{\partial \xi_2}\frac{S_2}{S}\Big) \end{aligned} \tag{19}$$

Equation (19) requires the evaluation of the velocity derivatives. These are computed by following equations (11), and (9).

2.2.1 κ-ω Turbulence Models

The transport equation for the turbulent specific dissipation ω is not integrated in the first cell close to a solid boundary but its value is directly imposed as

$$\omega^+ = \sqrt{(\omega_{log}^{+^2} + \omega_{visc}^{+^2})} \tag{20}$$

with ω^+_{log}, and ω^+_{visc}, the solution of ω in the log and viscous layer, given by

$$\omega^+_{log} = \frac{1}{\sqrt{\beta^*}}\frac{1}{\kappa_a}\frac{1}{\xi_2^+} \qquad \omega^+_{visc} = \frac{6}{\beta \xi_2^{+^2}} \tag{21}$$

where β^* and β are the constants of the $\kappa - \omega$ model. The value of ω is computed by

$$\omega^+ = \frac{\omega \nu}{u_\omega^2} \tag{22}$$

with $u_\omega = \max\left[u_\tau, u^*\right]$, where $u_\tau = \sqrt{u^2_{\tau,1} + u^2_{\tau,2} + u^2_{\tau,3}}$ is evaluated by equation (9), and u^* is given by (6).

2.2.2 κ-ε Turbulence Model

The value of ε in the first cell close to a solid boundary is computed following equation (20) and by considering that

$$\varepsilon = \beta^* \omega \kappa \tag{23}$$

2.2.3 Spalart-Allmaras Turbulence Model

The working variable of the Spalart-Allmaras turbulence model $\tilde{\nu}$ is computed by considering a direct dependence on the distance inside the logarithmic region of the boundary layer

$$\tilde{\nu}^+ = \frac{\tilde{\nu}}{\nu} = \kappa_a \xi_2^+ \tag{24}$$

It is worth noting that equation (6) cannot be used for the iterative solution of (4). The initial value of the distance is assumed to be $\tilde{\xi}_2$.

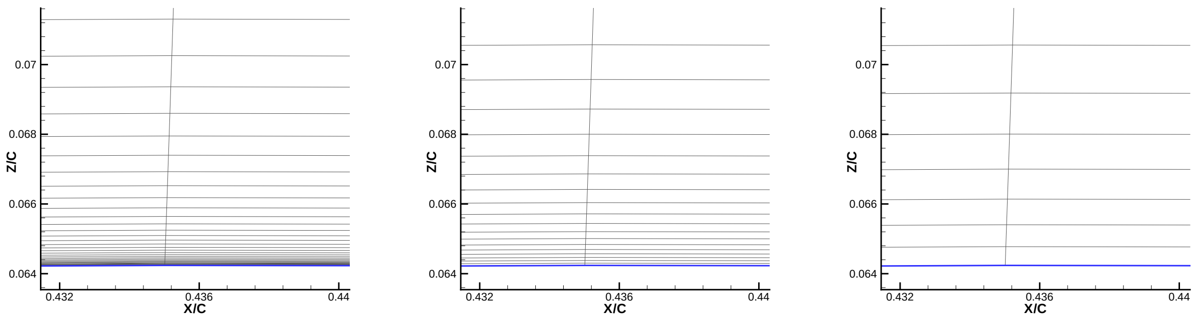

(a) Grid 0 (b) Grid 1 (c) Grid 2

Figure 1: Spacing of the grids in the wall-normal direction

3. Results ans Discussion

The formulation detailed in the previous section has been implemented in the CIRA flow solver ZEN. ZEN is a multi-block very robust, efficient and well assessed computational tool for the analysis of complex configurations in the subsonic, transonic, and supersonic regimes [4]. The equations are discretized by means of a cell-centred finite volume scheme with blended self adaptive second and fourth order artificial dissipation. The time-accurate version of the flow solver [10] makes use of the dual-time stepping procedure. The dual-time relaxations are performed by the Runge-Kutta algorithm with local time stepping and residual averaging, on different grid levels. The multigrid scheme is used to accelerate the convergence of the solution. Algebraic, one-equation, two-equations [2], and non linear eddy viscosity turbulence models [1] are available.

The wall functions have been already applied, in conjunction with the κ-ω TNT [9] turbulence model, to high lift flows [5]. Transonic applications are discussed in this paper. Four turbulence models (Spalart-Allmaras [13], $\kappa-\varepsilon$ Myong-Kasagi [12], κ-ω TNT [9] and SST [11]) have been applied to simulate the flow around the RAE 2822 airfoil, and the wing RAE M2155 placed in a wind tunnel [3]. The resutls obtained by the wall functions are compared to wall-integared simulations and experimental data [14].

3.1 RAE 2822 Airfoil

A structured multi-block grid with 335 points (261 on the body and 37 on the wake) in the stream-wise and 81 points in the wall-normal direction has been generated. Starting form this mesh, two other grids have been obtained by increasing the height of the wall-adjacent cells. In order to save the distribution law of the points, the number of cells in the wall-normal direction has been decreased. The characteristics of the grids are summarized in the table 1. Fully

Table 1: Charcteristics of the grids

Grid	Height of the wall-adjacent cells	Number of cells in the wall-normal direction
0	5×10^{-6}	80
1	6×10^{-5}	64
2	5×10^{-4}	52

turbulent flow conditions have been assumed.

3.1.1 Case 10

The case 10 flow condition has the following specification [8]:

- $Mach\ \ number = 0.754$, $Reynolds\ \ number = 6.2 \times 10^6$, $\alpha = 2.57°$

The flow is characterized by a shock-induced separation followed by a pressure recovery and a re-attachment.

The pressure and friction coefficients computed by applying the set of turbulence models on the three grids considered are shown in figure 2 and 3 respectively. The results obtained by applying standard no-slip boundary

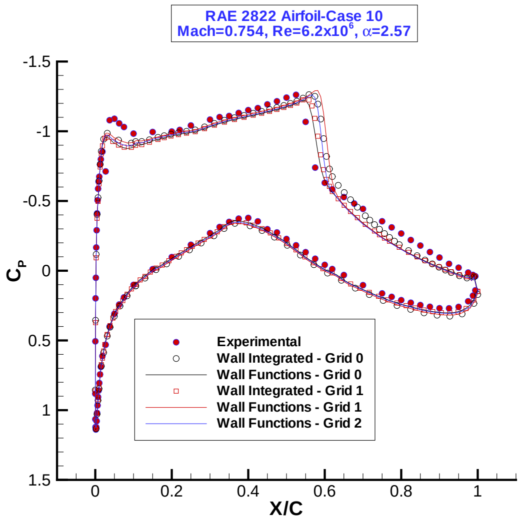

(a) κ-ε Myong-Kasagi

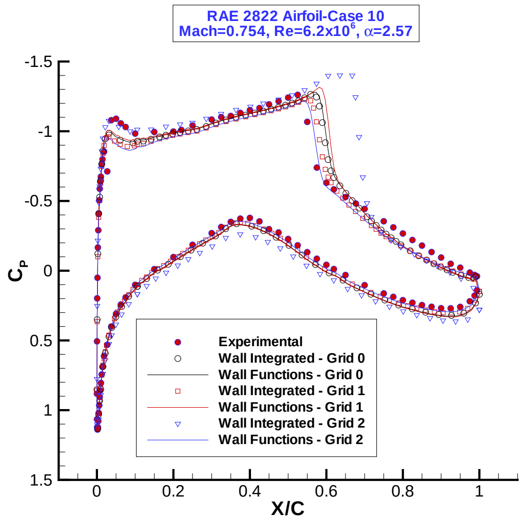

(b) Spalart-Allmaras

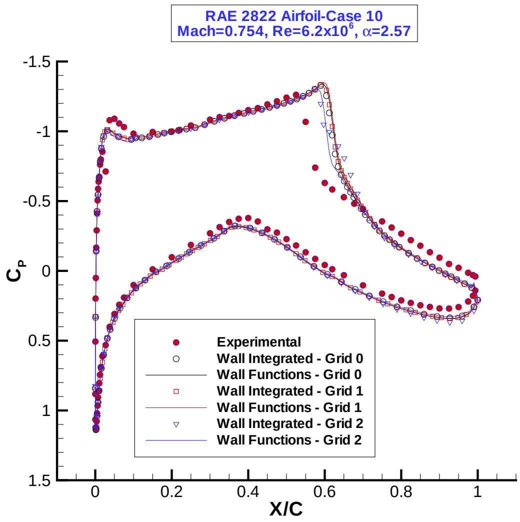

(c) κ-ω TNT

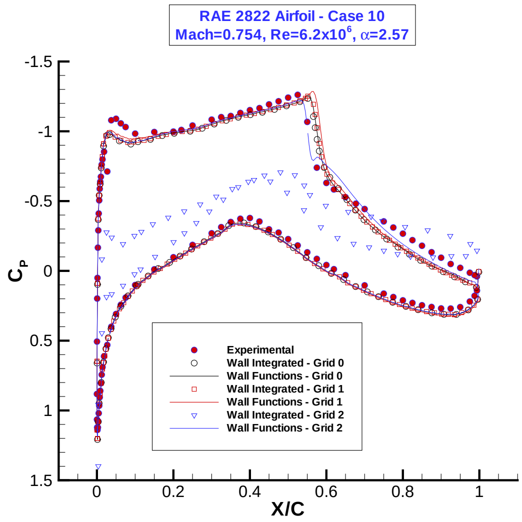

(d) κ-ω SST

Figure 2: RAE 2822 case 10 - Pressure Coefficient

conditions are poor on grid 2. This is particularly evident for the κ-ω SST turbulence model. The results obtained by the κ-ω SST on grid 2 are not satisfactory even when the wall functions are applied. A step in the C_p is visible just downstream the shock. This reflects in a too much large separated zone as can be clearly noted in figure 3.

The friction coefficients (figure 3) computed by the wall functions show a flow separation on all the grids. The re-attachment is returned by all the turbulence models except the Spalart-Allmaras. The level of the friction coefficient in the recovery region is quite good for both the TNT and SST κ-ω models. The error in the C_F with respect to the wall integrated simulation on grid 0 seems acceptable for all the turbulence models. The κ-ε and κ-ω models provide on grid 2 a friction coefficient with a transition-like behaviour in the front part of the airfoil.

Profiles of the streamwise velocity have been analyzed at three different stations in order to assess how the wall functions reproduce details of the flow field (figures 4-7). The results are discussed with reference to the experimental data and wall integrated results obtained on grid 0. The first station ($x/c = 0.40$) is located upstream the shock in an accelerating flow region, the second station is just downstream the shock where the flow should be separated, and the last station is inside a region of pressure recovery. The velocity profile obtained by wall integrating the RANS equations are very well reproduced on the coarse grid by the wall functions applied with the Spalart Allmaras, and $\kappa - \omega$ models. The SST $\kappa - \omega$ provide an excellent result also on grid 1. It is worth noting that at the station $x/c = 0.65$,

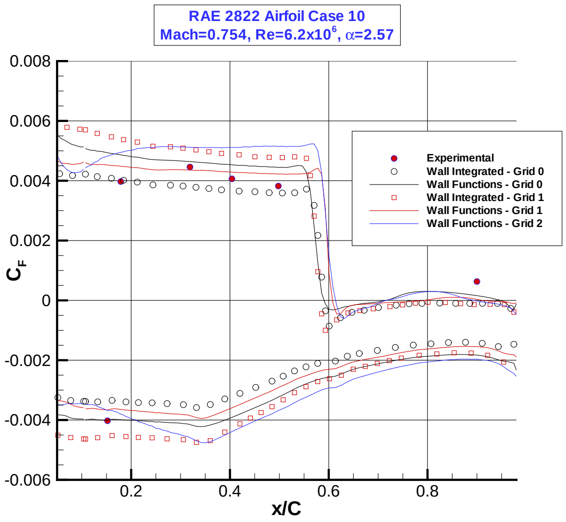

(a) κ-ε Myong-Kasagi

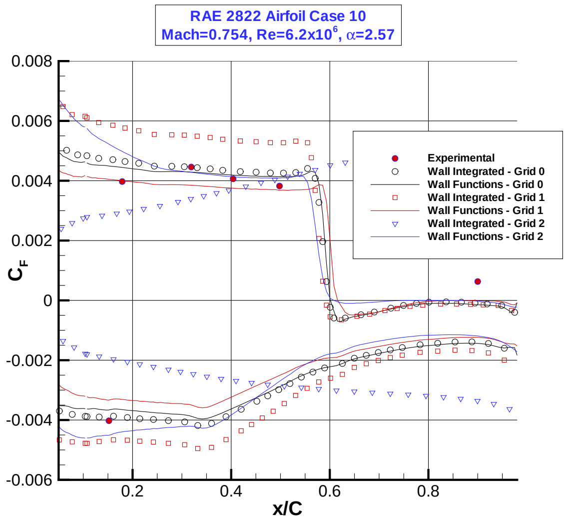

(b) Spalart-Allmaras

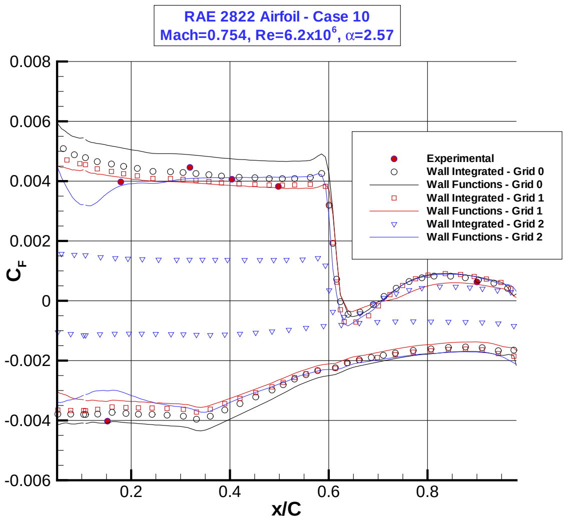

(c) κ-ω TNT

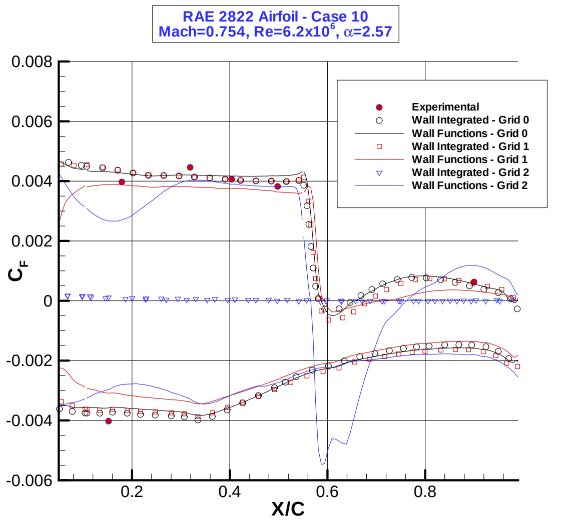

(d) κ-ω SST

Figure 3: RAE 2822 case 10 - Friction Coefficient

some discrepancies can be noted very close to the wall, because some solutions provide an attached flow. At the stations $x/c = 0.90$, the best result is provided by the $\kappa - \omega$ models as could be anticipated also by the plot of the friction coefficient. The poor result returned by the wall functions applied with the SST $\kappa - \omega$ on grid 2 can be noted in the velocity profiles. The too large separated region is quite evident at the station $x/c = 0.65$, and the subsequent too strong pressure recovery is visible on the results at $x/c = 0.90$.

3.2 RAE M2155 Wing

The flow around the wing RAE M2155 has been cosidered as a 3D transonic application. The case 2 condition :

- $Mach\ \ number = 0.806$, $Reynolds\ \ number = 4.1 \times 10^6$, $\alpha = 2.50°$

is characterized by a quite complex topology. The flow on the upper surface of the wing is characterized by a triple shock wave system from the root to about the 50% of the span, and by a single shock wave from about the 50% to the tip. Inboard the 50% span, changes in the flow direction occur in the region of the forward leg of the triple shock

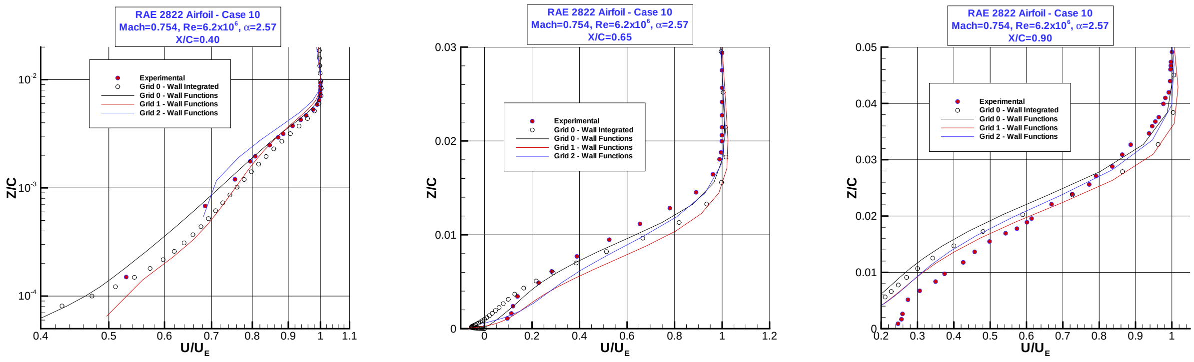

(a) $X/C = 0.40$ (b) $X/C = 0.65$ (c) $X/C = 0.90$

Figure 4: RAE 2822 case 10 - Velocity Profiles -$\kappa - \varepsilon$

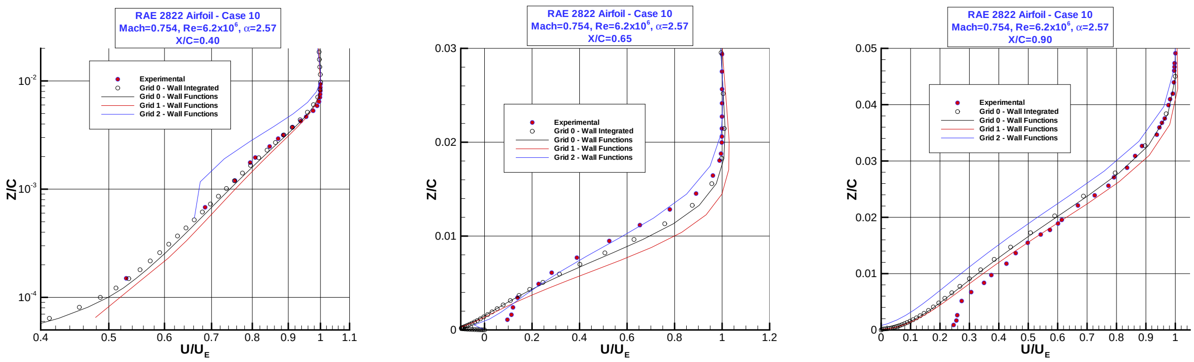

(a) $X/C = 0.40$ (b) $X/C = 0.65$ (c) $X/C = 0.90$

Figure 5: RAE 2822 case 10 - Velocity Profiles - Spalart- Allmaras

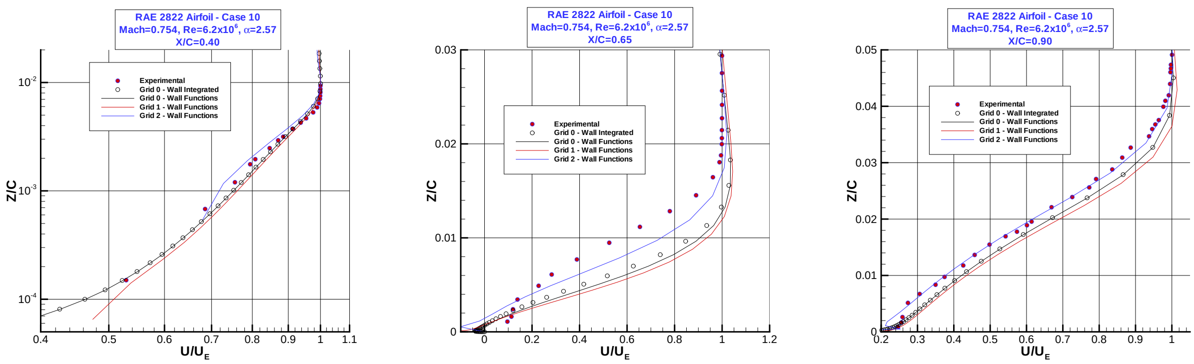

(a) $X/C = 0.40$ (b) $X/C = 0.65$ (c) $X/C = 0.90$

Figure 6: RAE 2822 case 10 - Velocity Profiles - $\kappa - \omega$ TNT

wave system and in trailing edge zone but without flow separation. The flow separation starts where the three shock waves join together and ends at about 90% of the span. The separation extends for about 10% of the local chord. A mesh with 35 blocks has been employed. A fine and a coarse version of the grid has been used. The fine has about 1.2×10^6 cells and values of y^+ of order of magnitude 1. The coarse mesh has been obtained by deleting 12 grid lines in the wall normal direction in the blocks surrounding the body, and the y^+ of the first layer of cells has been increased of more than one order of magnitude (figure 8). The $\kappa - \varepsilon$ Myong-Kasagi, Spalart-Allmaras, TNT and SST $\kappa - \omega$ have been applied with standard no-slip boundary conditions and the wall functions on both the fine and coarse version of

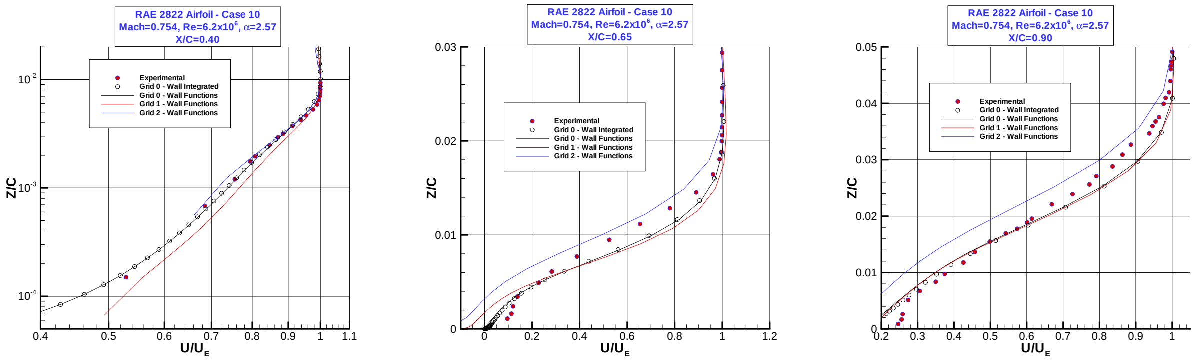

(a) $X/C = 0.40$ (b) $X/C = 0.65$ (c) $X/C = 0.90$

Figure 7: RAE 2822 case 10 - Velocity Profiles - $\kappa - \omega$ SST

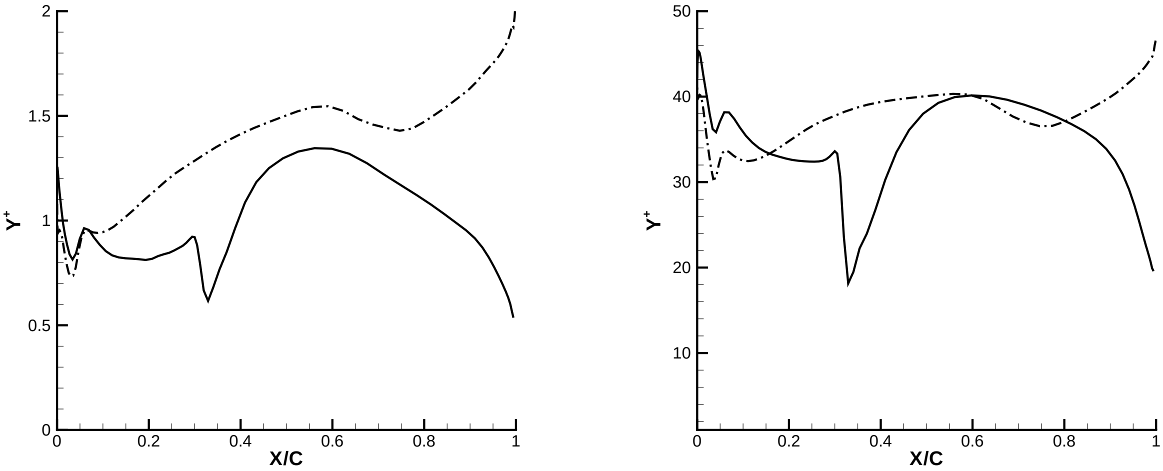

(a) Fine grid (b) Coarse grid

Figure 8: Wing RAE M2155 - y^+ Distribution at the station $2y/b = 0.5$

the grid.

The results in terms of pressure coefficient obtained at several stations along the span of the wing are shown in the figures 9 and 10. The dependence of the shock location on the y^+ is always weak and more evident in the wall integrated results. This is more appreciable for the second shock at the inboard sections where the triple shock-wave system is present (figure 9). The wall functions provide a good result on either the fine and coarse grid except when applied with the SST $\kappa - \omega$ model. This model provides a poor result when used with the wall function formulation on the fine grid. On the other hand, the C_P obtained by wall integrating the NS equations on the fine grid is reproduced in excellent way by the SST $\kappa - \omega$ when the wall functions are used on the coarse mesh. In the wing sections where a flow separation is present (figure 10), the wall integrated pressure coefficient obtained on the coarse grid by the $\kappa - \omega$ and $\kappa - \varepsilon$ models show a discrepancy with the experimental data downstream the shock. The Spalart-Allmaras turbulence model provide a similar C_P on both the grids either when no-slip boundary conditions and the wall functions are applied.

The aerodynamic coefficients obtained in all the simulations performed are summarized in the table 2. The drag coefficient has been split in the pressure and friction contribution in order to better assess the influence of the wall functions on the skin friction distribution. The results obtained by wall-integrating the RANS equations on the fine grid are considered as the "exact" numerical values. The data are presented in terms of percentage errors, and, as expected, the most sensitive parameter is the C_{D_f}. The coefficients provided by the wall funtions are reasonable on both the coarse and fine grid. The poor result provided by the SST κ-ω with the wall functions on the fine mesh is clearly reflected in the aerodynamic coefficients. The Spalart-Allmaras and the TNT κ-ω provide the "best" results on the fine

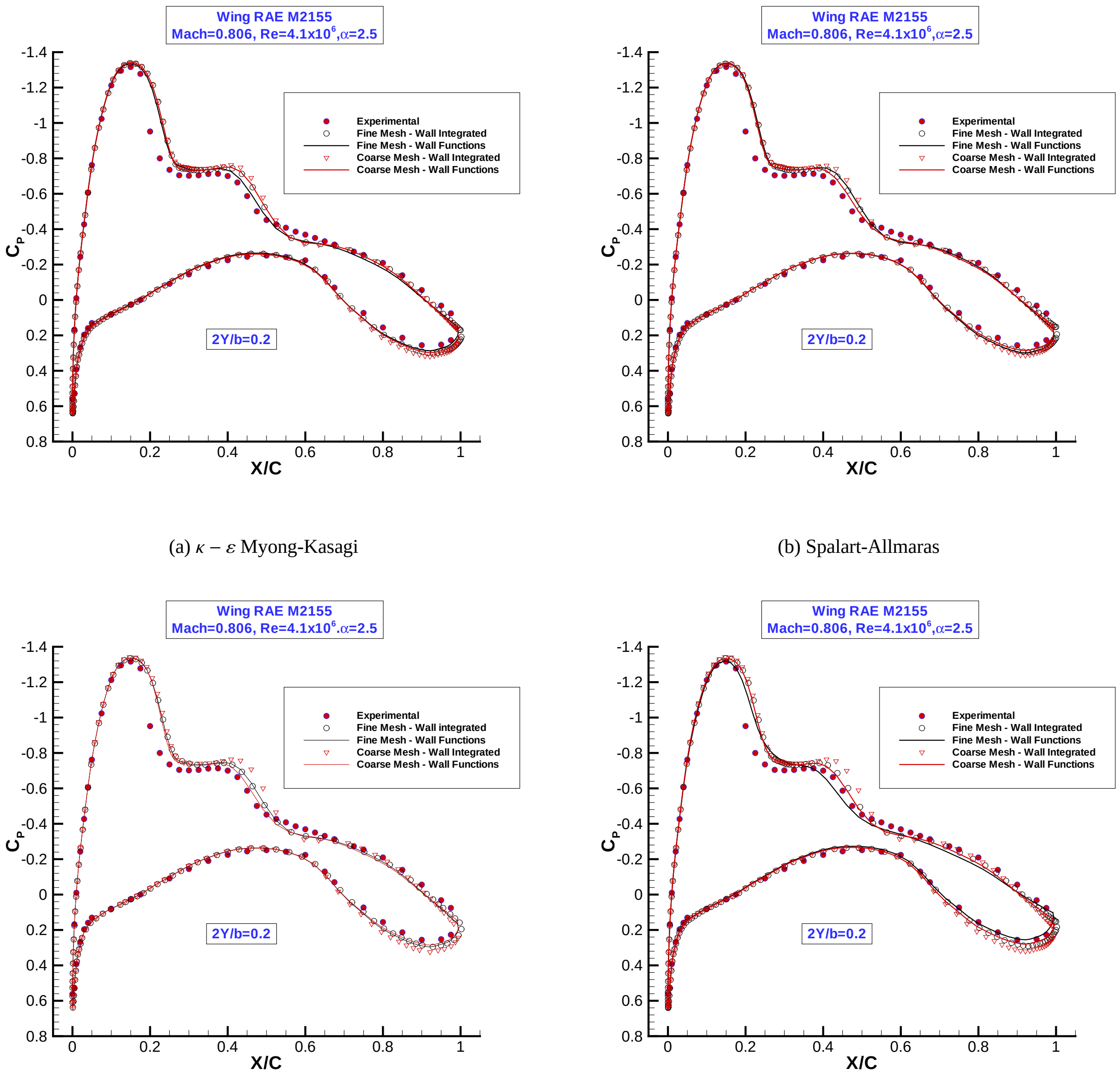

(a) $\kappa - \varepsilon$ Myong-Kasagi

(b) Spalart-Allmaras

(c) $\kappa - \omega \quad TNT$

(d) $\kappa - \omega \quad SST$

Figure 9: Wing RAE M2155 : Pressure Distribution - $2y/b = 0.2$

grid. The wall-integrated simulations on the coarse grid over-estimate the pressure contributions of the coefficients and largely under-estimate the friction drag. The percentage error in the friction drag coefficient is generally halved on the coarse grid by applying the wall functions. This is not true for the Spalart-Allmaras model that provides the same error (in absolute value) but the wall function over-estimate and the wall integrated under-estimate the C_{D_f}.

4. Conclusions

A wall functions formulation has been implemented in the CIRA flow solver ZEN, and tested for transonic flows. The RAE 2822 airfoil and the wing RAE M2155 placed in a wind tunnel have been considered. Both the applications represent a severe test case for the wall functions. A strong boundary layer interaction with an induced separation is present. A pressure recovery with a flow re-attachment occurs in the trailing-edge zone.

Fine meshes with values of y^+ about 1, and grids expressly generated by increasing the height of the wall-adjacent layers of cells have been considered. Wall functions and no-slip boundary conditions have been applied on both the kind of grids. This has allowed to assess the accuracy and the scalability with the grid-spacing of the formulation.

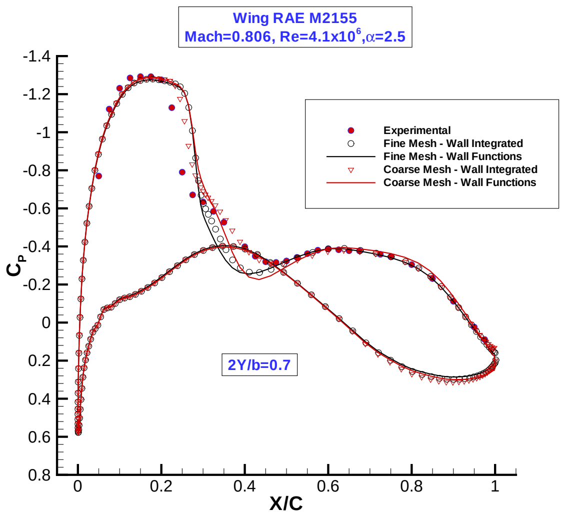

(a) $\kappa - \varepsilon$ Myong-Kasagi

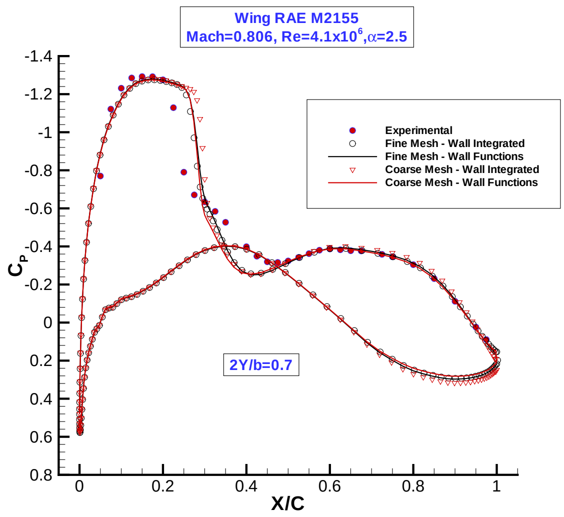

(b) Spalart-Allmaras

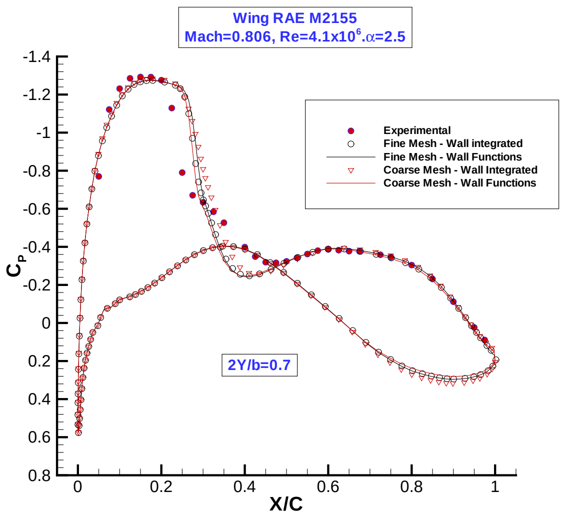

(c) $\kappa - \omega \quad TNT$

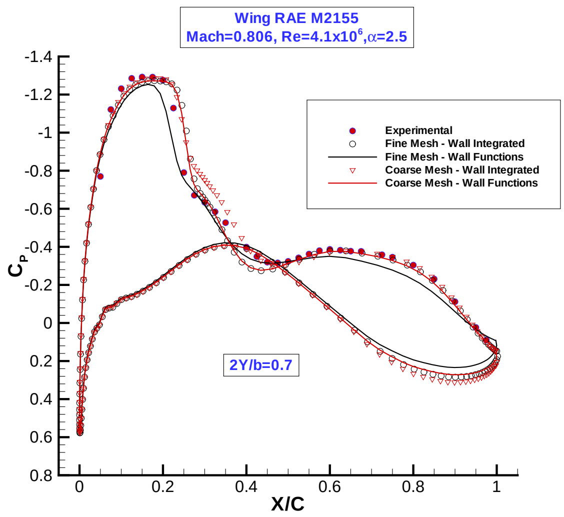

(d) $\kappa - \omega \quad SST$

Figure 10: Wing RAE M2155 : Pressure Distribution - $2y/b = 0.7$

Moreover it has been possible to evaluate the robustness of the numerical method used.

The wall functions have returned satisfactory results. The flow separations and re-attachments have been predicted with a good accuracy. The wall functions have generally enhanced the robustness of the numerical method allowing for grids with large values of the y^+ of the wall-adjacent layer of cells. Care has to be taken in applying the wall functions with the κ-ω SST model. This seems to be related to the boundary condition used for the ω equation. It has been shown that the wall functions can be applied on fine grids with very good values of y^+ and on coarse grids with higher values of y^+. The Spalart-Allmaras is the turbulence model, between the four models considered, that has shown less dependency on y^+.

5. Acknowledgments

The work presented in this paper has been performed within the project ACADEMIA (Advanced Computational Aerodynamic Design Environment for Multidisciplinary Integrated Analysis) partially funded by the Italian Ministry of University and Scientific Research.

Table 2: Percentage error of the Aerodynamic Coefficients

	Wall Functions					
	Fine Mesh			**Coarse Mesh**		
Turbulence Model	C_L	C_{D_p}	C_{D_f}	C_L	C_{D_p}	C_{D_f}
Myong-Kasagi $\kappa - \varepsilon$	4.35	4.51	6.35	0.64	0.35	12.70
Spalart-Allmaras	0.90	0.00	3.28	1.70	1.76	14.75
TNT $\kappa - \omega$	0.95	0.35	1.61	2.10	2.48	19.35
SST $\kappa - \omega$	10.30	5.78	40.00	2.23	1.44	18.18
	Wall Integrated					
	Fine Mesh			**Coarse Mesh**		
Turbulence Model	C_L	C_{D_p}	C_{D_f}	C_L	C_{D_p}	C_{D_f}
Myong-Kasagi $\kappa - \varepsilon$	0.00	0.00	0.00	1.08	0.69	26.98
Spalart-Allmaras	0.00	0.00	0.00	3.37	2.11	14.75
TNT $\kappa - \omega$	0.00	0.00	0.00	4.25	3.55	37.10
SST $\kappa - \omega$	0.00	0.00	0.000	4.76	4.33	29.09

References

[1] Amato, M. and Catalano, P. Non Linear κ-ε turbulence modeling for industrial applications. In *ICAS 2000 Congress*, September 2000

[2] Catalano, P. and Amato, M. Assessment of κ-ω turbulence modeling in the CIRA flow solver ZEN. In *3rd ECCOMAS Computational Fluid Dynamics Conference*, September 2001

[3] Catalano P., Amato M. A numerical evaluation of 2-D and 3-D application challenges of transonic aerodynamics by applying different turbulence models. *QNET-CFD Network Newsletter*, 1:25-28, 2001

[4] Catalano P., Amato M. An evaluation of RANS turbulence modelling for aerodinamic applications. *Aerospace science and Technology*, 7:493-509, 2003

[5] Catalano P., Vitagliano P. L. A Scalable Wall Functions Approach for High Reynolds Number Flows. In *1st European Conference for AeroSpace Sciences*, July 2005

[6] Craft T.J., Gerasimov A.V., Iacovides H., Launder B.E. Progress in the generalization of wall-function treatments. *International Journal of Heat and Fluid Flow*, 23:148-160, 2002

[7] Grotjans H., Menter F. Wall functions for general application CFD codes. In *4th ECCOMAS European Computational Fluid Dynamics Conference*, pages 1112–1117, 1998

[8] Haase W., Bradsma F. Elsholz E., Leschziner M., Schwamborn D. EUROVAL - An European initiative on validation of CFD codes. *Notes on Numerical Fluid Mechanics*, 42, 1992

[9] Kok J. C. Resolving the dependence on free-stream values for the κ-ω turbulence model. *AIAA Journal*, 38:1292-1295, 2000

[10] Marongiu, C., Catalano, P., Amato, M., and Iaccarino, G. U-ZEN : A computational tool solving U-RANS equations for industrial unsteady applications. *AIAA Paper 2004-2345*, July 2004

[11] Menter F. R. Two equation eddy viscosity turbulence models for engineering applications. *AIAA Journal*, 32:1598-1605, 1994.

[12] Myong H., Kasagi N. A new approach to the improvement of the $\kappa - \varepsilon$ turbulence model for wall bounded shear flows. *JSME International Journal*, 33:63-72, 1990.

[13] Spalart P. R., Allmaras S. R. A one equation turbulence model for aerodynamics flows. AIAA paper 92-0439, 30th Aerospace Science Meeting and Exhibit, January 6-9 1992, RENO, USA

[14] AGARD. Experimental data base for computer program assessment Agard Advisory Report 138, North Atlantic Treaty Organization, 7 Rue Ancelle, 92200 Neuilly-sur-Seine, France, may 1979.

eucass

This page has been purposedly left blank